

08,10

Hopping conductivity in multilayer nanostructures

$\{[(\text{Co}_{40}\text{Fe}_{40}\text{B}_{20})_{34}(\text{SiO}_2)_{66}]/[\text{ZnO}]\}_n$

© Yu.E. Kalinin¹, A.V. Sitnikov¹, V.A. Makagonov^{1,¶}, V.A. Foshin¹, M.N. Volochaev^{2,3}

¹Voronezh State Technical University,
Voronezh, Russia

²Kirensky Institute of Physics, Federal Research Center KSC SB, Russian Academy of Sciences,
Krasnoyarsk, Russia

³Siberian State University of Science and Technology,
Krasnoyarsk, Russia

¶E-mail: vlad.makagonov@mail.ru

Received November 12, 2024

Revised November 13, 2024

Accepted November 13, 2024

The structure and electrical properties of multilayer thin films $\{[(\text{Co}_{40}\text{Fe}_{40}\text{B}_{20})_{34}(\text{SiO}_2)_{66}]/[\text{ZnO}]\}_n$ with different thickness of ZnO interlayers are studied. It was found that the $(\text{Co}_{40}\text{Fe}_{40}\text{B}_{20})_{34}(\text{SiO}_2)_{66}$ composite interlayers are amorphous, and the ZnO interlayers are hexagonal crystalline with the structure of $P6_3mc$ symmetry group. The temperature dependence of the specific electrical resistance of multilayer nanostructures $\{[(\text{Co}_{40}\text{Fe}_{40}\text{B}_{20})_{34}(\text{SiO}_2)_{66}]/[\text{ZnO}]\}_n$ at the temperature range of 80–280 K obeys the „1/4“ law, which is interpreted as Mott type hopping conductivity along the ZnO interlayers. In this case, the dependence of specific electrical resistance of the reference zinc oxide films at the noted temperatures is described by the logarithmic law $\rho(T) \propto \ln T$, which indicates the presence of interference effects. The reference nanocomposites demonstrates the „1/2“ mechanism, which is explained within the framework of the Efros–Shklovsky conductivity mechanism models and thermally activated tunneling. The effective density of electron states of multilayer nanostructures $\{[(\text{Co}_{40}\text{Fe}_{40}\text{B}_{20})_{34}(\text{SiO}_2)_{66}]/[\text{ZnO}]\}_n$ nonlinearly increases with increasing zinc oxide layer thickness, which is associated with the presence of a thin layer of ZnO oxidized during the deposition process at the composite-ZnO interfaces.

Keywords: multilayer nanostructures, electrical resistance, hopping conductivity, density of electron states.

DOI: 10.61011/PSS.2024.11.60096.305

1. Introduction

Currently, there is still interest in studying the structure, morphology, and physical properties of heterogeneous metal-dielectric nanocomposites and multilayer structures based on them [1–3]. The practical interest in heterogeneous nanostructures is associated with the fact that composites with ferromagnetic granules are characterized by the presence of a gigantic magnetoresistance [4–6], reaching 8% at room temperature [7], the anomalous Hall effect [8], high values of the magnetorefractive effect [9,10], the Kerr effect [11,12], as well as the presence of memristive properties in them [13,14]. Moreover, a nanostructured multilayer heterogeneous material with magnetic inclusions should have the effects of magnetic proximity and exchange interaction between the layers, which is determined by the morphology of the heterogeneous system and the structure of the interface between different phases [15,16].

There is a large number of known studies of the mechanisms of electrical transfer in nanocomposites. The electrical properties of nanogranulated composites radically depend on the ratio of the metallic and dielectric phases in the material. There are two fundamentally different modes

of conductivity in composites, determined by the volume ratio of the dielectric and metallic phases and, accordingly, the structure of the material: the metallic mode and the nonmetallic mode [17,18].

The non-metallic conduction mode is realized when the volume fraction of the metallic phase in the composite is less than the percolation threshold. The structure of such a material consists of metal nanogranules electrically isolated from each other, separated by dielectric layers. The dielectric mode is characterized by high values of electrical resistivity, decreasing by several orders of magnitude with an increase of the proportion of metal in the composite to the percolation threshold. The electrical resistance of composites increases in case of cooling and the change ρ reaches several orders of magnitude in the temperature range of 4.2–300 K.

The hopping mechanism of conductivity dominates in a broad temperature range since the metallic phase in such heterogeneous systems is separated by layers of the dielectric phase [19–21]. At the same time, a hopping conductivity mechanism is usually implemented in granular metal-dielectric composites in the low temperature region in localized states near the Fermi level with a variable hopping range according to „1/4“ Mott’s law) [22]. The

dominant mechanism can dramatically change when obtaining a multilayer structure based on a granular metal-dielectric composite with different layers. Thus, the presence of a carbon interlayer in a multilayer nanostructure $[(\text{Co}_{40}\text{Fe}_{40}\text{B}_{20})_{34}(\text{SiO}_2)_{66}/\text{C}]_{47}$ containing 47 bilayers results in the fact that the electrical resistance changes to a hopping mechanism in accordance with „ $1/2$ “ Efros–Shklovsky law, and the characteristic temperature linearly depends on the thickness of the carbon layer [23].

Recent studies of the effect of the thickness of the ZnO semiconductor layer on the structure, magnetic, magneto-optical properties and magnetoresistance of multilayer nanostructures $\{[(\text{Co}_{40}\text{Fe}_{40}\text{B}_{20})_{34}(\text{SiO}_2)_{66}]/[\text{ZnO}]\}_n$ (where n is the number of bilayers in the film), showed an increase of the magneto-optical Kerr effect and magnetoresistance compared with a pure composite $(\text{Co}_{40}\text{Fe}_{40}\text{B}_{20})_{34}(\text{SiO}_2)_{66}$ [24]. In particular, the magnetoresistance of multilayer nanostructures in 10 kO field at 300 K reaches 4% at room temperature and 12% at 77 K, which is close to record values for nanocomposites. At the same time, the mechanisms of electronic transport in the studied multilayer nanostructures have not been widely discussed.

The electrical properties of multilayer nanostructures $\{[(\text{Co}_{40}\text{Fe}_{40}\text{B}_{20})_{34}(\text{SiO}_2)_{66}]/[\text{ZnO}]\}_n$ with different thickness of zinc oxide interlayers were studied in this paper.

2. Samples and experimental methods

Multilayer nanostructures $\{[(\text{Co}_{40}\text{Fe}_{40}\text{B}_{20})_{34}(\text{SiO}_2)_{66}]/[\text{ZnO}]\}_n$ were obtained by the ion-beam sputtering in an argon atmosphere with a purity of 99.998%, followed by deposition on substrates alternately occupying the positions of deposition of composite and ZnO according to the procedure described in Ref. [25–27] while the substrate holder rotated around the axis of the evaporation chamber. The vacuum chamber was vacuumed to the limit pressure of the residual gases equal to $P = 64$ MPa before sputtering. Composite layers were sputtered using a composite target made of $\text{Co}_{40}\text{Fe}_{40}\text{B}_{20}$ metal alloy with thirteen plates of SiO_2 evenly distributed on its surface (see a composite target diagram in Ref. [28]). This configuration of the composite target was selected specifically in order to obtain a composite composition $(\text{Co}_{40}\text{Fe}_{40}\text{B}_{20})_{34}(\text{SiO}_2)_{66}$, i.e. up to the percolation threshold, with a high content of metal phases. A ceramic zinc oxide target was used to obtain ZnO interlayers. A V-shaped screen was installed between the ZnO target and the substrate during deposition, which made it possible to adjust the thickness of the semiconductor layer in the range of 2–4 nm.

The V-shaped screen was not used when sputtering the composite interlayers, which made it possible to obtain the thickness of the composite interlayer of ~ 1 –1.5 nm. The number of bilayers n was 50, which was determined by a trade-off between the deposition duration and the film thickness. Thus, the final formula of

the obtained multilayer nanostructures can be written as $\{[(\text{Co}_{40}\text{Fe}_{40}\text{B}_{20})_{34}(\text{SiO}_2)_{66}]/[\text{ZnO}]\}_50$.

Composite $(\text{Co}_{40}\text{Fe}_{40}\text{B}_{20})_{34}(\text{SiO}_2)_{66}$ and ZnO films were separately synthesized on a „rotating substrate“ using a V-shaped screen to determine the optimal conditions for obtaining multilayer nanostructures with layers of the order of several nanometers. The thickness values of the composite $(\text{Co}_{40}\text{Fe}_{40}\text{B}_{20})_{34}(\text{SiO}_2)_{66}$ and ZnO films measured at several points of the substrate holder by optical interferometry were divided by the number of revolutions of the substrate holder, which gave preliminary values of the thicknesses of composite $(\text{Co}_{40}\text{Fe}_{40}\text{B}_{20})_{34}(\text{SiO}_2)_{66}$ and ZnO interlayers, which were expected to be obtained in a multilayer nanostructure. The exact thicknesses of the composite and ZnO interlayers in the multilayer nanostructure were determined by X-ray diffraction in the region of small Bragg angles and transmission electron microscopy.

Polycrystalline glass plates (ST-50) were used as substrates for electrical, magnetic, magnetoresistive and magneto-optical measurements, as well as single-crystal silicon with orientation (001) for X-ray measurements and transmission electron microscopy.

The chemical composition of the films was studied using Oxford INCA Energy 250 EDX detector with JEOL JSM-6380 LV scanning electron microscope. The structure was studied by X-ray diffraction using Bruker D2 Phaser diffractometer ($\lambda_{\text{CuK}\alpha 1} = 1.54 \text{ \AA}$) with DIFFRAC software.EVA 3.0 with the ICDD PDF Release 2012 database. Cross-sectional micrography in a transmission electron microscope (TEM) and electron diffraction images were obtained using Hitachi HT7700 microscope at an accelerating voltage of 100 kV (source W). Cross sections with a thickness of about 40–50 nm were prepared using a focused ion beam system (FIB, Hitachi FB2100). The sample was pre-coated with an amorphous germanium protective film to protect the films from destruction during the preparation of the cross-section.

The dependences of electrical resistivity were measured by a direct current two-probe method using a universal digital multimeter B7–78/1 along the plane of the film and layers of the multilayer structure.

3. Experimental results and their discussion

3.1. Structure of films

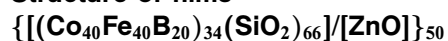


Figure 1 shows X-ray diffraction patterns from multilayer nanostructures $\{[(\text{Co}_{40}\text{Fe}_{40}\text{B}_{20})_{34}(\text{SiO}_2)_{66}]/[\text{ZnO}]\}_50$ with different thicknesses of ZnO interlayers, nanocomposite $(\text{Co}_{40}\text{Fe}_{40}\text{B}_{20})_{34}(\text{SiO}_2)_{66}$ and ZnO films obtained by deposition on a rotating substrate. The analysis of the provided X-ray patterns showed that the composite layers in the multilayer structure, as well as the reference composite $(\text{Co}_{40}\text{Fe}_{40}\text{B}_{20})_{34}(\text{SiO}_2)_{66}$, have an amorphous structure,

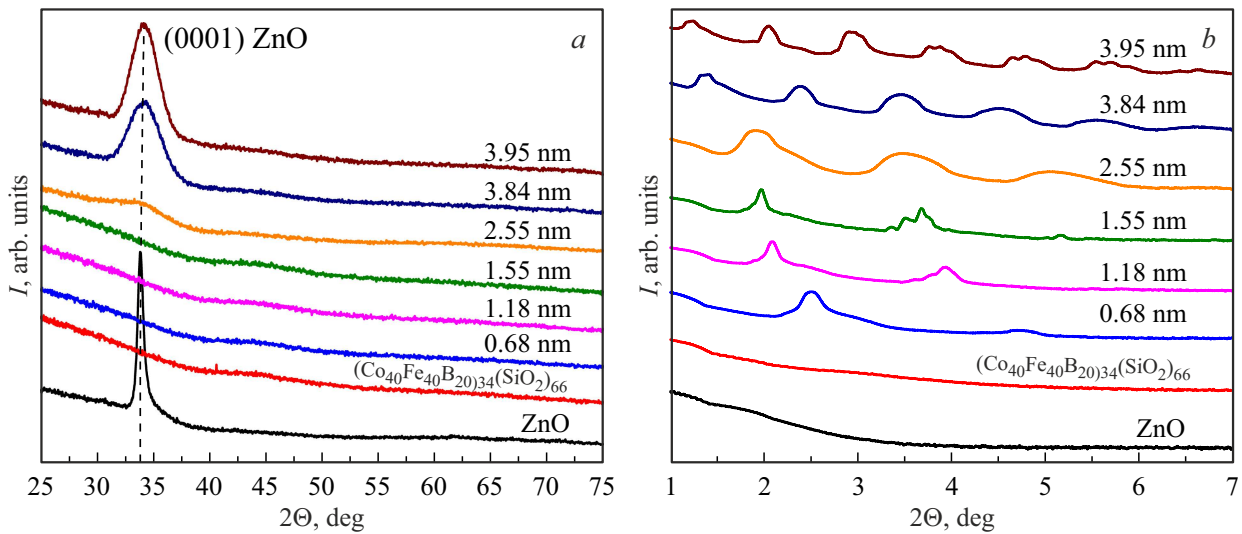


Figure 1. X-ray diffraction patterns of ZnO, composite $(\text{Co}_{40}\text{Fe}_{40}\text{B}_{20})_{34}(\text{SiO}_2)_{66}$ films and multilayer nanostructures of $\{[(\text{Co}_{40}\text{Fe}_{40}\text{B}_{20})_{34}(\text{SiO}_2)_{66}]/[\text{ZnO}]\}_n$ with different thickness of ZnO interlayers, measured at medium (a) and small (b) Bragg angles. The figures for the curves show the thicknesses of ZnO interlayers in multilayer nanostructures of $\{[(\text{Co}_{40}\text{Fe}_{40}\text{B}_{20})_{34}(\text{SiO}_2)_{66}]/[\text{ZnO}]\}_n$.

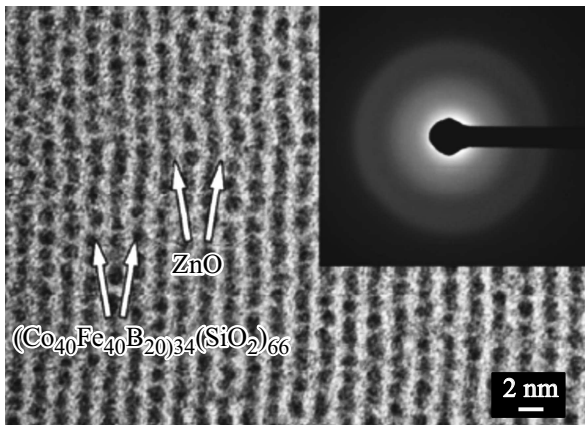


Figure 2. Microimage of a cross-section of a multilayer structure $\{[(\text{Co}_{40}\text{Fe}_{40}\text{B}_{20})_{34}(\text{SiO}_2)_{66}]/[\text{ZnO}]\}_n$, obtained using TEM (the insert shows the diffraction pattern of the studied film).

and the ZnO interlayers have a hexagonal crystal structure with the symmetry group $P63mc$ (Figure 1, a) [29]. It should be noted that the diffraction pattern of the ZnO film is characterized by the presence of a narrow diffraction maximum at $2\theta \approx 34^\circ$ (Figure 1, a), which can be classified as a peak (0001) of hexagonal cell of ZnO. The increase of the thickness of ZnO interlayers in a multilayer structure $\{[(\text{Co}_{40}\text{Fe}_{40}\text{B}_{20})_{34}(\text{SiO}_2)_{66}]/[\text{ZnO}]\}_n$ leads to an increase of the intensity of the diffraction peak ZnO (0001), but its width is significantly larger than the observed width of pure ZnO. The presence of only one reflection peak is attributable to the strong texture. That being said, it appears that the crystalline structure of ZnO is not formed in case of small thicknesses of the interlayers.

X-ray diffraction in the region of small Bragg angles ($2\theta = 1-7^\circ$) revealed the presence of diffraction peaks in all the studied multilayer nanostructures $\{[(\text{Co}_{40}\text{Fe}_{40}\text{B}_{20})_{34}(\text{SiO}_2)_{66}]/[\text{ZnO}]\}_n$ (Figure 1, b), which can be interpreted as the presence of a multilayer structure.

Diffraction studies using transmission electron microscopy (TEM) confirmed the amorphous structure of the constituent layers of the film with a small thickness of the ZnO interlayer (insert in Figure 2), and micrographs of the cross-section of the system $\{[(\text{Co}_{40}\text{Fe}_{40}\text{B}_{20})_{34}(\text{SiO}_2)_{66}]/[\text{ZnO}]\}_n$ confirmed the formation of composite interlayers $(\text{Co}_{40}\text{Fe}_{40}\text{B}_{20})_{34}(\text{SiO}_2)_{66}$ and a multilayer structure (Figure 2), while the thickness of the interlayers in the studied sample $(\text{Co}_{40}\text{Fe}_{40}\text{B}_{20})_{34}(\text{SiO}_2)_{66}$ was 1.1 nm, and the thickness of ZnO interlayers was 1.2 nm.

3.2. Electrical properties of multilayer nanostructures $\{[(\text{Co}_{40}\text{Fe}_{40}\text{B}_{20})_{34}(\text{SiO}_2)_{66}]/[\text{ZnO}]\}_n$

3.2.1. Temperature dependences of the electrical conductivity of reference composite films $(\text{Co}_{40}\text{Fe}_{40}\text{B}_{20})_{34}(\text{SiO}_2)_{66}$ and ZnO

Figure 3 shows the temperature dependences of the electrical resistivity of composite $(\text{Co}_{40}\text{Fe}_{40}\text{B}_{20})_{34}(\text{SiO}_2)_{66}$ (a) and zinc oxide ZnO (b) films obtained on a „rotating substrate“ over 100 deposition cycles during passage of the substrate in the temperature range of 80–280 K in the target sputtering zone. An increase of the film thickness is accompanied by a decrease of the electrical resistivity over the entire temperature range studied for both the composite $(\text{Co}_{40}\text{Fe}_{40}\text{B}_{20})_{34}(\text{SiO}_2)_{66}$ and ZnO.

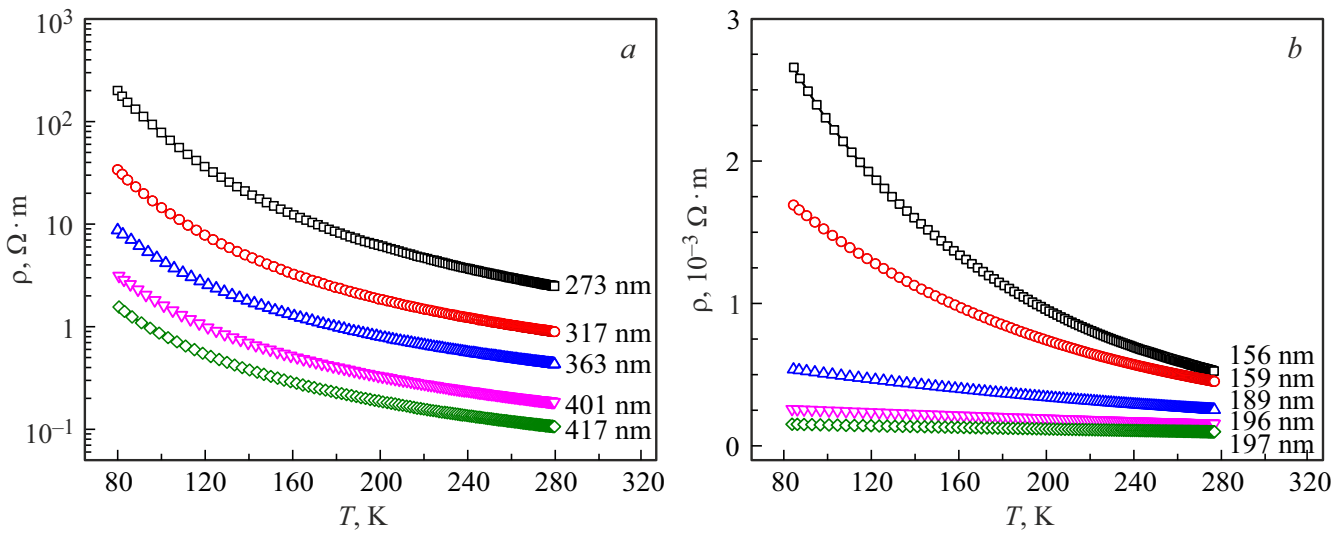


Figure 3. Temperature dependences of the electrical resistivity of composite films $(\text{Co}_{40}\text{Fe}_{40}\text{B}_{20})_{34}(\text{SiO}_2)_{66}$ (a) and ZnO (b) of different thicknesses (indicated next to the curves).

A decrease of electrical resistivity with the increase of temperature is observed both for composite $(\text{Co}_{40}\text{Fe}_{40}\text{B}_{20})_{34}(\text{SiO}_2)_{66}$ (Figure 3, a) and for zinc oxide films (Figure 3, b) of different thicknesses, while the temperature coefficient of resistance increases for both composite and ZnO films with the decrease of the thickness. The observed patterns can be related to both the impact of surface conditions and/or the additional oxidation of films during the passage of substrates outside the deposition zone.

The obtained dependences of the electrical resistivity of the composite $(\text{Co}_{40}\text{Fe}_{40}\text{B}_{20})_{34}(\text{SiO}_2)_{66}$ were analyzed in accordance with the equation:

$$\rho(T) = \rho_0(T) \exp[(T_0/T)]^p, \quad (1)$$

where $\rho_0(T)$ — temperature-dependent pre-exponential multiplier T , T_0 — characteristic temperature, $p = 1$ for the nearest neighbor conductivity mechanism [30], $p = 1/4$ for hopping conductivity with the Mott-type variable hopping range [31] and $p = 1/2$ in the case of Efros–Shklovsky type variable hopping range [32]. The experimental results of electrical resistivity were analyzed by linearization of the experimental dependences in the appropriate coordinates, assuming that the preexponential multiplier $\rho_0(T)$ in the formula (1) is weakly dependent or almost independent on the temperature. Figure 4 shows that the temperature dependences of the electrical resistivity are straightened in coordinates $\ln \rho \propto f(T^{-1/2})$ in the temperature range of 80–280 K. This dependence can be explained within the framework of the thermally activated electron tunneling models proposed in the studies of Sheng and Abeles [33], or a hopping conductivity mechanism with a variable hopping range of the Efros–Shklovsky type.

It should be noted that the characteristic temperature is determined by the following expression for Efros–Shklovsky

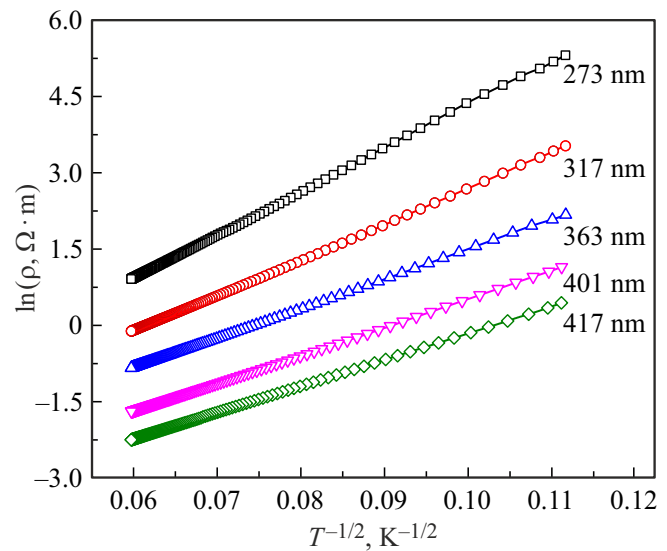


Figure 4. Temperature dependences of electrical resistivity, represented in coordinates $\ln \rho \propto f(T^{-1/2})$ for composite films $(\text{Co}_{40}\text{Fe}_{40}\text{B}_{20})_{34}(\text{SiO}_2)_{66}$ of different thicknesses (indicated next to curves).

type variable hopping range:

$$T_{0\text{SE}} = \frac{C_1 e^2}{4\pi \epsilon_0 \epsilon a k_B}, \quad (2)$$

where $C_1 = 2.8$, e — electron charge, ϵ_0 — electrical constant, ϵ — dielectric constant of the medium, a — radius of localization of the wave function, k_B — Boltzmann constant.

The radius of localization of the wave function a can be estimated knowing the Efros–Shklovsky characteristic

Parameters of Efros–Shklovsky-type variable hopping range models calculated from experimental dependences at $T = 100$ K and Sheng–Abeles thermally activated tunneling model

Thickness of film, nm	$T_{0\text{ES}}$, K	a , nm	R_{ES} , nm	W_{ES} , meV	Δ , meV	C , meV
273	7197.9	1.3	2.8	36.6	73.2	155
317	4780.8	1.9	3.4	29.8	59.6	103
363	3317.9	2.8	4.05	24.8	49.6	71
401	2957.3	3.2	4.3	23.4	46.8	64
417	2680.8	3.5	4.5	22.3	44.6	58

temperature $T_{0\text{ES}}$ from expression (2):

$$a = \frac{C_1 e^2}{4\pi\epsilon_0\epsilon k_B T_{0\text{se}}}. \quad (3)$$

We use the value of the dielectric constant $\epsilon = 4$ given for silicon oxide according to the data provided in Ref. [34] to estimate a . The obtained values of the radius of localization of the wave function are shown in the table.

The values of the average range R_{ES} and the hopping energy W_{ES} can be estimated substituting the obtained values a using the formulas [30]:

$$R_{\text{SE}} = \frac{1}{4} a \left(\frac{T_{0\text{SE}}}{T} \right)^{1/2}, \quad (4)$$

$$W_{\text{SE}} = \frac{1}{2} k_B T \left(\frac{T_{0\text{SE}}}{T} \right)^{1/2}. \quad (5)$$

Assuming that the Coulomb gap is „soft“, i.e. the density of states vanishes at only one point, we obtain estimates of the width of the Coulomb gap, which can be approximately considered equal to twice the hopping energy (table). The obtained values of the Coulomb gap width are in agreement with the values obtained for the compound $\text{LaMnO}_{3+\delta}$ in Ref. [35].

Despite realistic estimates of parameters of Efros–Shklovsky-type variable hopping range for composite films $(\text{Co}_{40}\text{Fe}_{40}\text{B}_{20})_{34}(\text{SiO}_2)_{66}$, this model does not allow explaining the occurrence of giant magnetoresistance in both composite and multilayer nanostructures $\{[(\text{Co}_{40}\text{Fe}_{40}\text{B}_{20})_{34}(\text{SiO}_2)_{66}]/[\text{ZnO}]\}_{50}$ [24]. Therefore, we will evaluate the parameters of the Sheng and Abeles model for our results.

It is assumed in the thermally activated tunneling model that charge transfer is carried out by tunneling electrons directly from one granule to another through dielectric barriers in the same way as it occurs in case of tunneling through a thin dielectric layer between metal layers. Despite the fact that the tunneling is the mechanism of electrical transfer, only electrons that are thermally activated above the barrier caused by the Coulomb interaction (Coulomb

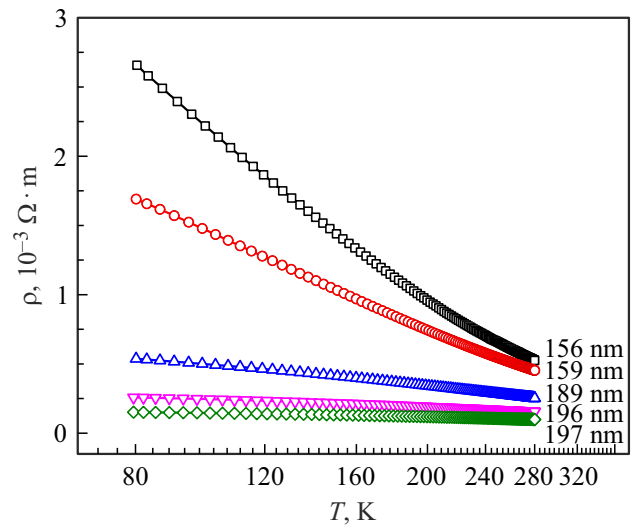


Figure 5. The temperature dependences of the electrical resistivity, represented in coordinates $\rho \propto f(\ln T)$ for ZnO films of different thicknesses (indicated next to the curves).

blockade phenomenon) can participate in this process. The dependences of the electrical resistivity of nanocomposites on temperature should be described by the following formula in this mode:

$$\rho = \rho_0 \left(\exp \left(2\sqrt{C/k_B T} \right) \right), \quad (6)$$

where

$$C = (4\pi/h)(2mU)^{1/2} s E_C,$$

— activation energy of the tunneling process, h — Planck’s constant, m — effective electron mass, U — effective barrier height, s — the width of the barrier equal to the shortest distance between the boundaries of the granules, E_C — Coulomb energy. Then, the activation energy of the tunneling process C can be determined by the angle of slope of the dependencies $\ln \rho \propto f(T^{-1/2})$. Estimates of the value of C are given in the table. The numerical values of C are in agreement with those given in the literature for composites Ni– SiO_2 , Au– Al_2O_3 , W– Al_2O_3 and Pt– SiO_2 are values for which the value of C is in the range of 0.004–0.3 eV [36].

Thus, it is not possible to unambiguously state which mechanism of electrical transfer, leading to a linear dependence $\ln \rho \propto f(T^{-1/2})$, is implemented in our case.

The analysis of the dependences of the electrical resistivity of ZnO films of different thicknesses (Figure 3, b) on the conformance with the mechanisms of electrical conductivity described by the formula (1) did not give a positive result, but a satisfactory linearization can be obtained if the obtained dependencies are rearranged in coordinates $\rho \propto f(\ln T)$ (Figure 5). The negative temperature coefficient of electrical resistivity may be associated in this case with the presence of weak localization of charge carriers, when a decrease of electrical resistivity is associated

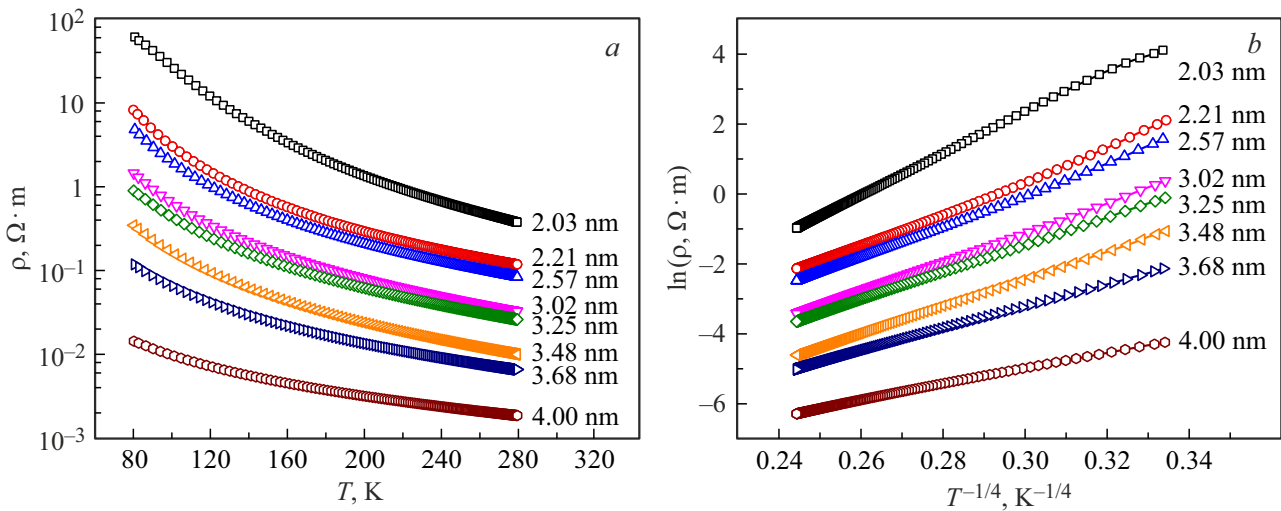


Figure 6. Temperature dependences of electrical resistivity, represented in coordinates $\rho \propto f(T)$ (a) and $\ln \rho \propto f(T^{-1/4})$ (b), multilayer nanostructures $\{[(\text{Co}_{40}\text{Fe}_{40}\text{B}_{20})_{34}(\text{SiO}_2)_{66}]/[\text{ZnO}]\}_{50}$ with different thickness of interlayers (indicated next to curves).

with quantum interference of wave functions of non-interacting electrons and an increasing role of interelectronic interaction [37].

3.2.2. Temperature dependences of electrical conductivity of multilayer nanostructures $\{[(\text{Co}_{40}\text{Fe}_{40}\text{B}_{20})_{34}(\text{SiO}_2)_{66}]/[\text{ZnO}]\}_{50}$

Temperature dependences of the electrical resistivity of multilayer nanostructures $\{[(\text{Co}_{40}\text{Fe}_{40}\text{B}_{20})_{34}(\text{SiO}_2)_{66}]/[\text{ZnO}]\}_{50}$, with different thickness of ZnO interlayers is shown in Figure 6, a.

The dominant mechanisms of electrical transfer of the studied films was determined by re-arranging the temperature dependences of the electrical resistivity in coordinates $\ln \rho \propto f(T^{-n})$, where n had the values of 1/4, 1/2, 1, $\ln \rho \propto f(\ln T)$. An analysis of the results showed that in the studied temperature range, the electrical resistivity is approximated by a straight line in the coordinates $\ln \rho \propto f(T^{-1/4})$ (Figure 6, b), which indicates the possibility of implementing Mott-type variable hopping range for localized states lying in a narrow energy band near the Fermi level [31].

If we interpret the fulfillment of the „law 1/4“ as a manifestation of Mott’s variable hopping range, then the expression for conductivity has the following form [31]:

$$\sigma = e^2 R_M^2 \nu_{\text{ph}} g(E_F) \exp\left(-\frac{T_{0M}}{T}\right)^{1/4}, \quad (7)$$

where

$$T_{0M} = \frac{C_2}{k_B g(E_F) a^3} \quad (8)$$

where $C_2 = 21$, e — electron charge, R_M — jump distance, ν_{ph} — phonon interaction spectrum factor, T — absolute temperature, $g(E_F)$ — density of states at the Fermi level,

a — radius of localization of the electron wave function, k_B — Boltzmann constant.

The values of T_{0M} were determined from Figure 6, b for the studied film compositions. Knowing T_{0M} , and assuming that the process of charge carrier transfer is limited by hops between metal granules of $\text{Co}_{40}\text{Fe}_{40}\text{B}_{20}$, we estimate the density of localized states by assuming a localization radius equal to the average size of the pellet in the composite (~ 1.5 nm), which corresponds to the thickness of the composite interlayer in a multilayer nanostructure.

We will also estimate the average hopping range, which for the case of Mott’s conductivity should be equal to

$$R_M = \frac{3}{8} a \left(\frac{T_{0M}}{T}\right)^{1/4} \quad (9)$$

and the energy of the charge carrier jump at a temperature of 100 K according to the formula

$$W_M = \frac{1}{4} k_B T \left(\frac{T_{0M}}{T}\right)^{1/4}. \quad (10)$$

The density of states, the average hopping range and hopping energy estimated in accordance with formulas (8)–(10) are shown in Figure 7.

As can be seen from Figure 7, the energy and average hopping range of charge carriers decrease with the increase of thickness of the zinc oxide ZnO layer, while the density of electronic states increases non-linearly. It should be noted that Mott’s variable hopping range was not detected in the reference films of the composite $(\text{Co}_{40}\text{Fe}_{40}\text{B}_{20})_{34}(\text{SiO}_2)_{66}$ and ZnO. The above-mentioned features of electrical transfer in multilayer nanostructures $\{[(\text{Co}_{40}\text{Fe}_{40}\text{B}_{20})_{34}(\text{SiO}_2)_{66}]/[\text{ZnO}]\}_{50}$, can be explained assuming that the conductivity is realized mainly by ZnO layers. As is known, oxygen vacancies are the main source

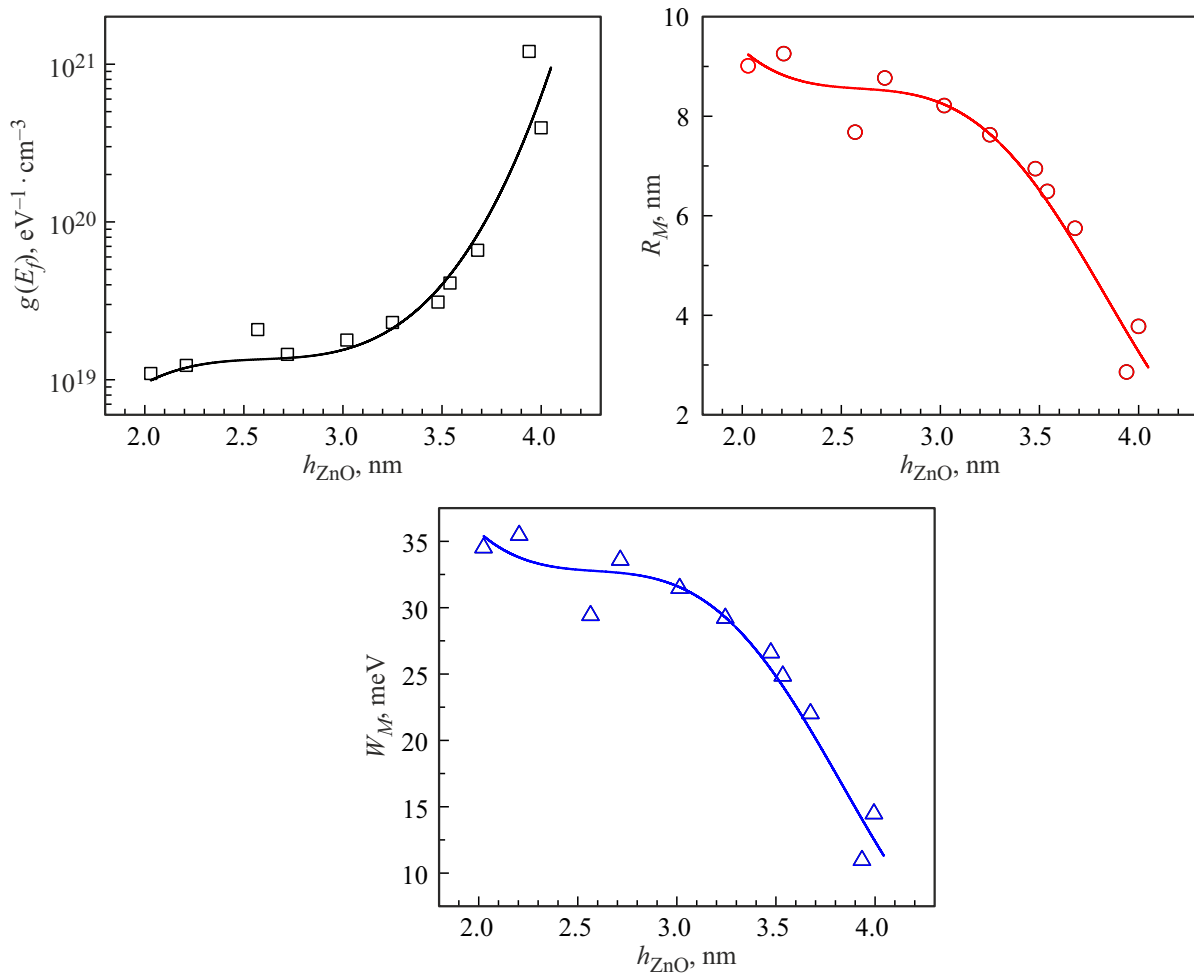


Figure 7. Parameters calculated according to models of hopping conductivity from the thickness of the zinc oxide interlayer.

of localized states in oxide semiconductors and dielectrics obtained by vacuum deposition methods. At the same time, taking into account the specific features of the method of synthesis of the studied multilayer structures, it is necessary to admit that the surface of the freshly sputtered layer is oxidized by the oxygen of residual gases when the substrate holder is moved from one deposition position (for example, ZnO) to another (composite). Since the oxygen diffusion coefficient in silicon oxide, which makes up the composite matrix $(\text{Co}_{40}\text{Fe}_{40}\text{B}_{20})_{34}(\text{SiO}_2)_{66}$, is significantly lower than in ZnO [38], then the oxygen of the residual gases penetrates mainly into ZnO.

ZnO layers with small thicknesses can be oxidized over the entire thickness, and the thinner the layer, the more oxygen it contains, and, consequently, the density of states in such layers is lower and weakly depends on the thickness. Only the surface layer of the interlayer is oxidized in a ZnO interlayer with a large thickness, and the „non-oxidized“ layer contains the maximum number of oxygen vacancies for these production conditions. The thickness of the „pre-oxidized“ layer practically does not change with a further increase of the thickness of the ZnO interlayers, and

the thickness of the „non-oxidized“ layer increases, which results in the electrical transfer over the „non-oxidized“ region of the ZnO interlayers and leads to a sharp increase of the effective density of states.

Thus, the estimates of the density of localized states shown in Figure 7 are averaged over the electric transfer channel in ZnO interlayers, and a violation of the conditions of quantum interference of wave functions observed for reference ZnO films (Figure 5) may be caused by an additional oxidation or a dimensional effect because of the small thickness of the interlayers. It should be noted that it is also impossible to deny the presence of electrical transfer through the composite layers $(\text{Co}_{40}\text{Fe}_{40}\text{B}_{20})_{34}(\text{SiO}_2)_{66}$, and the mechanism associated with them, which can also lead to nonlinear dependences of the density of localized states on the thickness of the ZnO interlayer.

4. Conclusion

Multilayer nanostructures {have been synthesized by ion beam sputtering of two targets (composite $\text{Co}_{40}\text{Fe}_{40}\text{B}_{20}$ with subsamples of SiO_2 and ceramic ZnO)

$\{[(\text{Co}_{40}\text{Fe}_{40}\text{B}_{20})_{34}(\text{SiO}_2)_{66}]/[\text{ZnO}]\}_{50}$, (where 50 is the number of bilayers in the film). The structure and electrical properties of synthesized films have been studied for the thicknesses of the ZnO semiconductor layer, varying from 2 to 4 nm. It has been established that the composite layers of the synthesized films have an amorphous structure, and the semiconductor layers of ZnO have a hexagonal crystal structure with a symmetry group $P63mc$. It is shown that the temperature dependence of the electrical resistivity of zinc oxide interlayers synthesized on a rotating substrate in the range of 80–280 K is described by the logarithmic law $\rho(T) \propto \ln T$, and by „1/2“ for nanocomposites $(\text{Co}_{40}\text{Fe}_{40}\text{B}_{20})_{34}(\text{SiO}_2)_{66}$, obtained on a rotating substrate.

The temperature dependence of specific gravity electrical resistance in the temperature range of 80–280 K obeys the law „1/4“ for multilayer films $\{[(\text{Co}_{40}\text{Fe}_{40}\text{B}_{20})_{34}(\text{SiO}_2)_{66}]/[\text{ZnO}]\}_n$, which is characteristic of Mott's variable hopping range in localized states near the Fermi level. It is found that the density of electronic states at the Fermi level increases non-linearly with the increase of the thickness of ZnO semiconductor interlayer.

Acknowledgments

The authors express their gratitude to the Center for Collective Use of the Federal Research Center „Krasnoyarsk Science Center of the Siberian Branch of the Russian Academy of Sciences“ (Krasnoyarsk) for conducting electron microscopic studies of samples.

Funding

This study was supported by the Russian Science Foundation (project No. 24-29-20099).

Conflict of interest

The authors declare that they have no conflict of interest.

References

- [1] E.P. Domashevskaya, S.A. Ivkov, A.V. Sitnikov, O.V. Stogney, A.T. Kozakov, A.V. Nikolsky, K.A. Barkov, N.S. Bulov. *J. Alloys Compd.* **870**, 159398 (2021). DOI: 10.1016/j.jallcom.2021.159398
- [2] S.A. Ivkov, K.A. Barkov, E.P. Domashevskaya, E.A. Ganshina, D.L. Goloshchapov, S.V. Ryabtsev, A.V. Sitnikov, P.V. Seregin. *Appl. Sci.* **13**, 5, 2992 (2023). DOI: 10.3390/app13052992
- [3] E.N. Sheftel, V.A. Tedzhetov, E.V. Harin, G.Sh. Usmanova. *Thin Solid Films* **748**, 139146 (2022). DOI: 10.1016/j.tsf.2022.139146
- [4] Z. Guo, S. Park, H.T. Hahn, S. Wei, M. Moldovan, A.B. Karki, D.P. Young. *Appl. Phys. Lett.* **90**, 053111 (2007). DOI: 10.1063/1.2435897
- [5] E.Z. Meilikhov, B. Raquet, H. Rakoto. *J. Exp. Theor. Phys.* **92**, 5, 816 (2001). DOI: 10.1134/1.1378173
- [6] J.V. Kasiuk, J.A. Fedotova, T.N. Koltunowicz, P. Zukowski, A.M. Saad, J. Przewoznik, Cz. Kapusta, J. Zukowski, I.A. Svito. *J. Alloys Compd.* **586** (1), S432 (2014). DOI: 10.1016/j.jallcom.2012.09.058
- [7] H. Fujimori, S. Mitani, S. Ohnuma. *Mater. Sci. Eng. B* **31**, 219 (1995). DOI: 10.1016/0921-5107(94)08032-1
- [8] H. Meier, M.Y. Kharitonov, K.B. Efetov. *Phys. Rev. B* **80**, 045122 (2009). DOI: 10.1103/PhysRevB.80.045122
- [9] A.B. Granovskii, E.A. Gan'shina, A.N. Yurasov, Yu.V. Boriskina, S.G. Yerokhin, A.B. Khanikaev, M. Inoue, A.P. Vinogradov, Yu.P. Sukhorukov. *J. Commun. Technol. Electron.* **52**, 1065 (2007). DOI: 10.1134/S1064226907090185
- [10] A.B. Granovsky, I.V. Bykov, E.A. Gan'shina, V.S. Gushchin, M. Inoue, Yu.E. Kalinin, A.A. Kozlov, A.N. Yurasov. *J. Exp. Theor. Phys.* **96**, 6, 1104 (2003). DOI: 10.1134/1.1591221
- [11] V.E. Buravtsova, E.A. Gan'shina, O.S. Ivanova, Yu.E. Kalinin, S.A. Kirov, S. Pkhongkhirun, A.V. Sitnikov. *Bull. Russ. Acad. Sci. Phys.* **71**, 1539 (2007). DOI: 10.3103/S1062873807110184
- [12] E.A. Gan'shina, V. Buravtsova, A. Novikov, Y. Kalinin, A.V. Sitnikov. *Solid State Phenom.* **190**, 361 (2012). DOI: 10.4028/www.scientific.net/SSP.190.361
- [13] A.V. Sitnikov, I.V. Babkina, Yu.E. Kalinin, A.E. Nikonov, M.N. Kopytin, K.E. Nikitin, K.Yu. Chernoglazov, S.N. Nikolaev, A.L. Vasiliev, A.V. Yemelyanov, V.A. Demin, V.V. Rylkov. *Nanoindustriya* **13**, s5-3(102), 687 (2020). (in Russian). DOI: 10.22184/1993-8578.2020.13.5s.687.696
- [14] A.I. Iliasov, A.N. Matsukatova, A.V. Emelyanov, P.S. Slepov, K.E. Nikiruy, V.V. Rylkov. *Nanoscale Horiz.* **9**, 2, 238 (2024). DOI: 10.1039/d3nh00421j
- [15] S.V. Komogortsev, E.A. Denisova, R.S. Iskhakov, A.D. Balaev, L.A. Chekanova, Yu.E. Kalinin, A.V. Sitnikov. *J. Appl. Phys.* **113**, 17C105 (2013). DOI: 10.1063/1.4794361
- [16] S.N. Nikolaev, K.Yu. Chernoglazov, A.V. Emelyanov, A.V. Sitnikov, A.N. Taldenkov, T.D. Patsaev, A.L. Vasiliev, E.A. Gan'shina, V.A. Demin, N.S. Averkiev, A.B. Granovsky, V.V. Rylkov. *JETP Lett* **118**, 1, 58 (2023). DOI: 10.1134/S0021364023601550
- [17] I.S. Beloborodov, A.V. Lopatin, V.M. Vinokur. *Phys. Rev. B* **72**, 125121 (2005). DOI: 10.1103/PhysRevB.72.125121
- [18] V.V. Rylkov, A.V. Emelyanov, S.N. Nikolaev, K.E. Nikiruy, A.V. Sitnikov, E.A. Fadeev, V.A. Demin, A.B. Granovsky. *JETP* **131**, 1, 160 (2020). DOI: 10.1134/S1063776120070109
- [19] Yu.E. Kalinin, A.N. Remizov, A.V. Sitnikov. *Phys. Solid State* **46**, 11, 2146 (2004). DOI: 10.1134/1.1825563
- [20] Yu.E. Kalinin, A.M. Kudrin, M.H. Piskareva, A.B. Sitnikov, A.K. Zvezdin. *Persp. Materialy* **3**, 41 (2007). (in Russian).
- [21] A.V. Sitnikov, V.A. Makagonov, Y.E. Kalinin, S.B. Kushchev, V.A. Foshin. *Tech. Phys.* **69**, 6, 1813 (2024). DOI: 10.1134/S1063784224060458
- [22] S.A. Gridnev, Yu.E. Kalinin, A.V. Sitnikov, O.V. Stogney. *Ne-lineynye yavleniya v nano- i mikroeterogennykh sistemakh. BINOM. Laboratoriya znaniy, M.* (2012). 352 p. (in Russian).
- [23] O.V. Gerashchenko, V.A. Ukleev, E.A. Dyad'kina, A.V. Sitnikov, Yu.E. Kalinin. *Phys. Solid State* **59**, 1, 164 (2017). DOI: 10.1134/S1063783417010073

- [24] Y.E. Kalinin, A.V. Sitnikov, V.A. Makagonov, V.A. Foshin, M.N. Volochaev, I.M. Pripechenkov, N.N. Perova, E.A. Ganshina, V.V. Rylkov, A.B. Granovsky. *J. Magn. Magn. Mater.* **604**, 172287 (2024). DOI: 10.1016/j.jmmm.2024.172287
- [25] O.V. Dunets, Y.E. Kalinin, M.A. Kashirin, A.V. Sitnikov. *Tech. Phys.* **58**, 9, 1352 (2013). DOI: 10.1134/S1063784213090132
- [26] M.N. Martyshev, A.V. Emelyanov, V.A. Demin, K.E. Nikiruy, A.A. Minnekhanov, S.N. Nikolaev, A.N. Taldenkov, A.V. Ovcharov, M.Yu. Presnyakov, A.V. Sitnikov, A.L. Vasiliev, P.A. Forsh, A.B. Granovsky, P.K. Kashkarov, M.V. Kovalchuk, V.V. Rylkov. *Phys. Rev. Appl.* **14**, 3, 034016 (2020). DOI: 10.1103/PhysRevApplied.14.034016
- [27] V.V. Rylkov, V.A. Demin, A.V. Emelyanov, A.V. Sitnikov, Yu.E. Kalinin, V.V. Tugushev, A.B. Granovsky. *Phys. Rev. B* **95**, 144402 (2017). DOI: 10.1016/B978-0-12-813594-5.00013-8
- [28] V.V. Rylkov, V.A. Demin, A.V. Emelyanov, A.V. Sitnikov, Yu.E. Kalinin, V.V. Tugushev, A.B. Granovsky. In: V. Domracheva, M. Capoli, E. Rentschler (Eds.), *Novel Magnetic Nanostructures: Unique Properties and Applications*, Elsevier, Amsterdam (2018), pp. 426–463. DOI: 10.1016/B978-0-12-813594-5.00013-8
- [29] A. Ashour, M.A. Kaid, N.Z. El-Sayed, A.A. Ibrahim. *Appl. Surf. Sci.* **252**, 22, 7844 (2006). DOI: 10.1016/j.apsusc.2005.09.048
- [30] V.F. Gantmacher. *Elektrony v neuporyadochennykh sredakh*. Fizmatlit, M. (2006). 232 p. (in Russian).
- [31] N. Mott, E. Davis. *Elektronnyye protsessy v nekrystallicheskiikh veshchestvakh: v 2 t.* Mir, M. (1982). 658 s. (in Russian).
- [32] B.I. Shklovsky, A.L. Efros. *Elektronnyye svoystva legirovannykh poluprovodnikov*. Nauka, M. (1979). 416 p. (in Russian).
- [33] P. Sheng, B. Abeles, Y. Arie. *Phys. Rev. Lett.* **31**, 1, 44 (1973). DOI: 10.1103/PhysRevLett.31.44
- [34] O. Madelung, U. Rössler, M. Schulz. *Landolt-Börnstein: Numerical Data and Functional Relationships in Science and Technology — New Series (LANDOLT 3, vol. 41D). Non-Tetrahedrally Bonded Binary Compounds II*. Springer-Verlag, Berlin Heidelberg (2000). XVIII, 535 p. DOI: 10.1007/b71139
- [35] V.S. Zakhvalinskiĭ, R. Laiho, K.G. Lisunov, E. Lähderanta, P.A. Petrenko, Yu.P. Stepanov, V.N. Stamov, M.L. Shubnikov, A.V. Khokhulin. *Phys. Solid State* **49**, 5, 918 (2007). DOI: 10.1134/S1063783407050198
- [36] B. Abeles, P. Sheng, M.D. Coutts, Y. Arie. *Adv. Phys.* **24**, 3, 407 (1975). DOI: 10.1080/00018737500101431
- [37] T.A. Polyanskaya, Yu.V. Shmartsev. *FTT* **23**, 1, 3 (1989). (in Russian).
- [38] G.V. Samsonov, A.L. Borisova, T.G. Zhidkova. *Physiko-khimicheskie svoystva okislov*. M.: Metallurgiya, (1978). 472 p. (in Russian).

Translated by A.Akhtyamov